ORIGINAL PAPER

RJME
Romanian Journal of Morphology & Embryology
http://www.rjme.ro/

Increased osteopontin expression and mitochondrial swelling in 3-nitropropionic acid-injured rat brains

HONG-LIM KIM[1,2)], BYUNG-JOON CHANG[1)], SUNG MIN NAM[1)], SANG-SOEP NAHM[1)], JONG-HWAN LEE[1)]

[1)]*Department of Anatomy, College of Veterinary Medicine and Veterinary Science Research Institute, Konkuk University, Seoul, Korea*

[2)]*Integrative Research Support Center, College of Medicine, Catholic University, Seoul, Korea*

Abstract

Osteopontin (OPN) is involved in the regulation of calcium precipitation in the brain pathology including ischemia. A 3-Nitropropionic acid (3NP) irreversibly inhibits mitochondrial complex II in the electron transport chain, with subsequent loss of transmembrane potential and calcium entry into the mitochondria. The present study examined the 3NP-induced calcium elevation in mitochondria and OPN expression in the 3NP-lesioned striatum. Rats were subcutaneously injected 3NP (15 mg/kg) every other day for six weeks. Histological analysis, including the Hematoxylin–Eosin, Nissl, and Alizarin Red S stainings, was performed to examine the neurotoxic effects of 3NP. The expression of OPN in the striatum of 3NP-treated rats was investigated with immunohistochemistry and immunoelectron microscopy. In the striatal lesions, extensive loss of neurons and white matter bundles was detected. OPN was mainly detected in the penumbra region of the 3NP lesion. Scattered OPN expression was colocalized in the striatal neurons. After Alizarin Red S staining, the increase of calcium deposition was detected in the striatal lesions. In the electron microscopic analysis, the localization of OPN was clearly observed in the ultrastructure of mitochondria by immunoperoxidase and immunogold-silver staining techniques. Taken together, present findings suggest that calcium-induced mitochondrial swelling is highly associated with OPN expression. Thus, striatal calcium accumulation may be derived from 3NP-induced alteration in mitochondrial calcium homeostasis and pathologically associated with the induction of OPN protein.

Keywords: calcium, mitochondrial swelling, 3-nitropropionic acid, osteopontin.

Introduction

Osteopontin (OPN) is a calcium-binding multi-functional protein containing an arginine-glycine-aspartate-binding integrin motif [1]. It is involved in numerous pathophysiological processes, including the inflammatory response [1], cell adhesion [2], wound repair [3], apoptosis [4], and tumor metastasis [5]. OPN is expressed in a variety of tissues, including bone, vascular tissue, kidney, and brain [6]. Recent studies have described the functions and characteristics of OPN in pathological brain conditions. Especially, OPN expression is associated with calcium precipitation in the ischemic lesion [7, 8]. Although OPN has been correlated with the calcium dyshomeostasis-induced cell degeneration, little is known about the underlying mechanisms of calcium accumulation in lesioned areas.

3-Nitropropionic acid (3NP), an irreversible inhibitor of mitochondrial complex II (succinate dehydrogenase), impairs energy metabolism which leads to subsequent neuronal cell death [9]. 3NP has been used to model Huntington's disease (HD) for its neurodegenerative effects on striatum replicating anatomical, histopathological, and neurochemical features of HD [10–12]. Specifically, the formation of nonselective mitochondrial permeability transition (MPT) pores is related with 3NP-induced neuro-degeneration [13, 14]. Excessive calcium in mitochondria allows opening of MPT pores with subsequent swelling, loss of membrane potential, and cytochrome c release [3, 15–17].

In our previous study, we reported that induction of OPN is associated with the mitochondrial dysfunction in 3NP-treated striatal neurons [18]. In the present study, we investigated the OPN expression, mitochondrial morphological changes, and calcium (Ca^{2+}) deposits in the 3NP-treated model.

Materials and Methods

Male Sprague–Dawley rats (n=10) weighing 300–320 g (9–10-week-old) were used. 3NP (Sigma-Aldrich Co., St. Louis, MO, USA) was dissolved in saline (pH 7.4). The animals were administered subcutaneous injections of 3NP (15 mg/kg) every other day for six weeks. Control rats (n=5) were subcutaneously administered the equivalent volume of saline. The animals were anesthetized with Chloral hydrate (400 mg/kg, intraperitoneal injection) and sacrificed two days after the final 3NP administration. All of the experimental procedures were conducted according to the guidelines of the Institutional Animal Care and Use Committee of Konkuk University (Seoul, Korea).

For histology, brain samples were removed, immersed in 4% paraformaldehyde for 12 hours, and then paraffin embedded. The brains were cut into 5-μm sections and then stained with Cresyl Violet (Nissl), Hematoxylin–Eosin (HE), and Alizarin Red S, in order to examine the histopathological changes. Tissue sections were selected from an area between 1.68 mm anterior and 1.56 mm posterior to the bregma.

For the immunochemical analysis of OPN in the striatal regions, brains were rapidly dissected into 2-mm-thick sections. The 2-mm-thick brain sections were treated with 0.3% hydrogen peroxide for quenching of endogenous peroxidase and then incubated in 1% bovine serum albumin (BSA) in 0.01 M phosphate-buffered saline (PBS) for two hours and then with a mouse monoclonal anti-OPN antibody (1:150 dilution, American Research Products, Inc., Waltham, MA, USA), at 4°C, overnight. The sections were washed three times for 10 minutes each in PBS, incubated for two hours in biotinylated goat anti-mouse IgG (1:400 dilution, Vector, Burlingame, CA, USA) and Streptavidin Peroxidase complex (1:400 dilution, Vector), at room temperature, and then washed three times for 10 minutes each with Tris buffer. The immunoreaction was visualized by using 3,3'-Diaminobenzidine (DAB) as the chromogen.

Additionally, the brain samples were cryoprotected and frozen in liquid nitrogen. For the immunofluorescence, semi-thin cryosections (1-μm thick) were cut at -80°C, on a Leica EM UC7 ultramicrotome equipped with a FC7 cryochamber. For the double-labeling studies, the brain sections were first incubated in blocking buffer (1% BSA) in PBS, in a dark humidified chamber for one hour, at room temperature and then in a mixture of the mouse monoclonal anti-OPN antibody (1:150 dilution, American Research Products, Inc., Waltham, MA, USA) plus rabbit polyclonal antibodies to dopamine and cyclic adenosine monophosphate (cAMP)-regulated neuronal phosphoprotein (DARPP-32, 1:100 dilution, Cell Signaling Technology, Inc., Danvers, MA, USA), at 4°C, overnight. The sections were washed three times for 5 minutes each in PBS and then incubated for two hours, at room temperature, with the following secondary antibodies: Cy3-conjugated donkey anti-mouse (1:2000 dilution, Jackson ImmunoResearch Laboratories, Inc., West Grove, PA, USA) and Alexa Fluor 488 goat anti-rabbit (1:300 dilution, Thermo Fisher Scientific, Inc., Waltham, MA, USA) for the OPN/DARPP-32 double labeling. Counter-staining of the cell nuclei was performed with 4',6-Diamidino-2-phenyindole (DAPI, 1:1000 dilution, Roche Diagnostics GmbH, Mannheim, Germany) for 10 minutes. The slides were examined and photographed with a confocal microscope (LSM 510 Meta, Carl Zeiss AG, Jena, Germany). Images were converted to *TIF* files, and the contrast levels were adjusted with Adobe Photoshop ver. 7.0 (Adobe Systems, Inc., San Jose, CA, USA).

For the immunoelectron microscopic analysis, pre-embedding immunoperoxidase methods were conducted. Fifty-μm-thick vibratome sections were selected and incubated in 1% BSA in 0.01 M PBS. Subsequently, sections were incubated with the mouse monoclonal anti-OPN antibody (1:150 dilution, American Research Products, Inc., Waltham, MA, USA), at 4°C, overnight. Sections were incubated with biotinylated goat anti-mouse IgG in 0.01 M PBS, at room temperature, for two hours, and reactions were visualized by using DAB as the chromogen. Then, they were post-fixed (1% Glutaraldehyde and 1% Osmium Tetroxide solution for 30 minutes each) and embedded in Epon 812 resin. After areas of interest were selected, excised and glued onto resin blocks, ultrathin sections (70–90 nm) were produced using an ultramicrotome. Following the staining with 1% Uranyl Acetate, sections were observed with an electron microscope (JEM 1010; JEOL, Ltd., Tokyo, Japan). Additionally, vibratome sectioning and primary antibody incubation were similarly conducted for immunogold-silver labeling. Next, sections were incubated with nanogold particles (1.4 nm) (1:100 dilution, Nanoprobes, Stony Brook, NY, USA) conjugated secondary antibody for two hours. After then, silver enhancement step was conducted using the HQ silver enhancement kit (Nanoprobes) for 3 minutes. Ultrathin sections were cut in the same condition and observed with an electron microscope.

A quantitative detection of OPN protein in mitochondria was performed by analyzing the immunogold/silver immunocytochemistry of OPN on the electron micrographs. The analysis was done on 150 mitochondria labeled with immunogold that were chosen randomly on ultrathin sections. Digital images of mitochondria that were taken with charge-coupled device (CCD) cameras attached to the electron microscope were loaded into ImageJ ver. 1.49 software and the real area of each mitochondria were calculated by applying the scale bar length with ImageJ. The mitochondria were classified according to their area size and the number of gold particles that were obtained by determining the average value of gold particles per 0.0625 μm^2 of each mitochondria.

The experimental data were analyzed by one-way analysis of variance (ANOVA), which were followed by *post-hoc* comparisons with Dunnett's test. *P*-values less than 0.05 were considered significant. The data are presented as mean ± standard error (SE).

Results

The morphology of the striata obtained from control and 3NP-treated rats were compared using Nissl and HE staining. Compared to the controls (Figure 1a), the cores of the 3NP lesions (Figure 1b) were pale in the Nissl-stained striatal sections. At higher magnification, the Nissl-stained 3NP lesions (Figure 1d) were characterized by marked neuronal loss in the striatum, whereas the controls (Figure 1c) did not show any discernible neuronal loss. The HE staining showed predominant white matter damage and cells with darkly stained nuclei, which may be involved in cell degeneration, in 3NP-lesioned striata (Figure 1f), and these were not observed in controls (Figure 1e). To investigate the calcium deposits in the 3NP-lesioned area, we performed Alizarin Red S staining. Positively stained calcium precipitates are characterized by orange-red color. In addition, the Alizarin Red S staining appeared stronger in the lesioned core than in other regions (Figure 5).

The OPN immunoperoxidase staining of the brain showed that immunoperoxidase labeling of OPN was not detected in the striatum of the control rat (Figure 2a). Whereas, the level of OPN protein was significantly elevated in the bilateral 3NP-induced striatal lesions (Figure 2b). Signal intensity was analyzed with black and white references of normal striatum and 3NP-injured striatum (Figure 2, a and b) by ImageJ program (left normal striatum: 0.138, right normal striatum: 0, left 3NP-injured striatum: 195.5, right 3NP-injured striatum: 162.28).

To identify whether the OPN protein is expressed in the striatal neurons, we conducted a double immunofluorescence staining of OPN and DARPP-32, which is a striatal neuron marker. OPN protein was not in the detectable level in the control rat striatum (Figure 3, a–c). However, OPN was expressed in the 3NP-treated striatum, double staining resulted a clear demarcation of lesion and penumbra region (Figure 3, d–f). Diffuse OPN immunolabeling, which appeared dot-like, was predominantly distributed in the lesioned core where DARPP-32 immunolabeling was absent. At a higher magnification, some OPN-immunoreactive dots in the penumbra were colocalized with DARPP-32 (Figure 3, g–i). These findings suggest that OPN expression was associated with the degeneration of the striatal neurons.

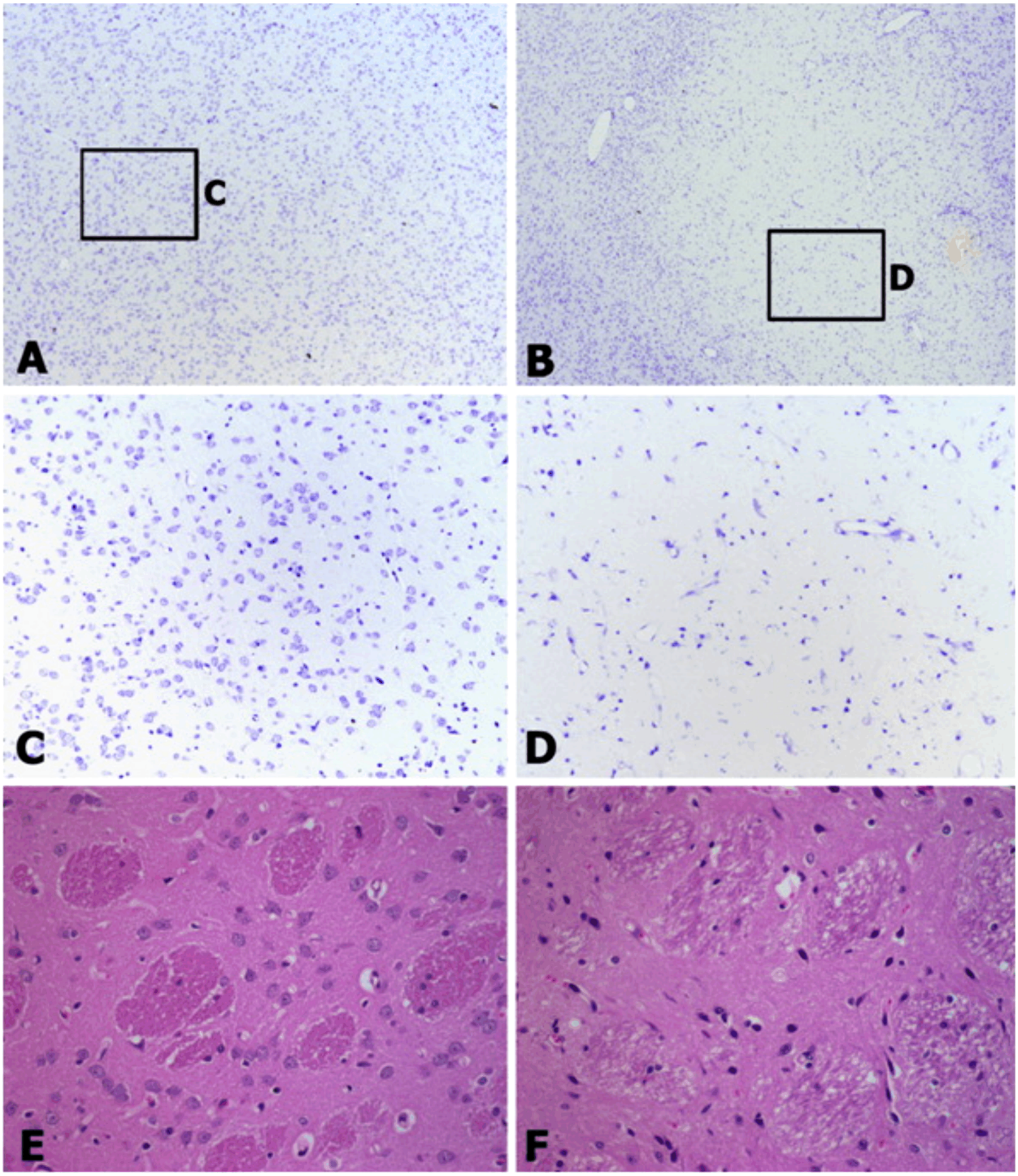

Figure 1 – ***Light micrographs of the Cresyl Violet (Nissl) and Hematoxylin–Eosin (HE) staining of the control brains and brains with 3-Nitropropionic acid (3NP)-injured striatum. The control section is evenly stained with Cresyl Violet (A), and the 3NP-injured lesion core is lightly stained (B). (C) Higher magnification of the boxed area in (A) shows a number of Cresyl Violet-stained neurons, whereas (D) the boxed area in (B) shows a loss of neurons. (E) The control group shows unaffected neuronal cells and normal white matter bundles on the HE-stained sections. (F) However, in the 3NP-injured lesion core, irregular and dark-stained nuclei and white matter bundle degeneration are detected. Nissl staining: (A and B) ×40; (C and D) ×200. HE staining: (E and F) ×400.***

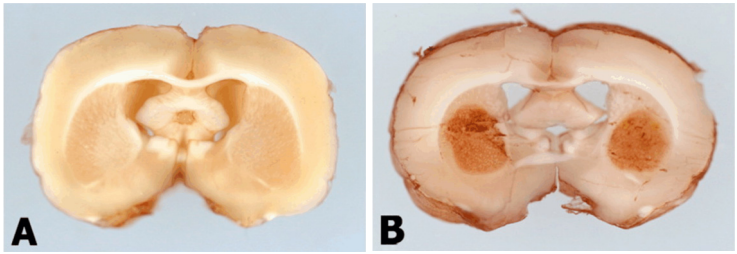

Figure 2 – ***Osteopontin (OPN) immunoperoxidase staining of the whole brain. Representative brain slices showing OPN immunoperoxidase immunocytochemistry in control rats that were treated with saline (A) and 3-Nitropropionic acid (3NP)-injured rats (B). OPN expression was observed in the bilateral striatum in the 3NP-injured rats, whereas no OPN expression was observed in the saline-treated control rats.***

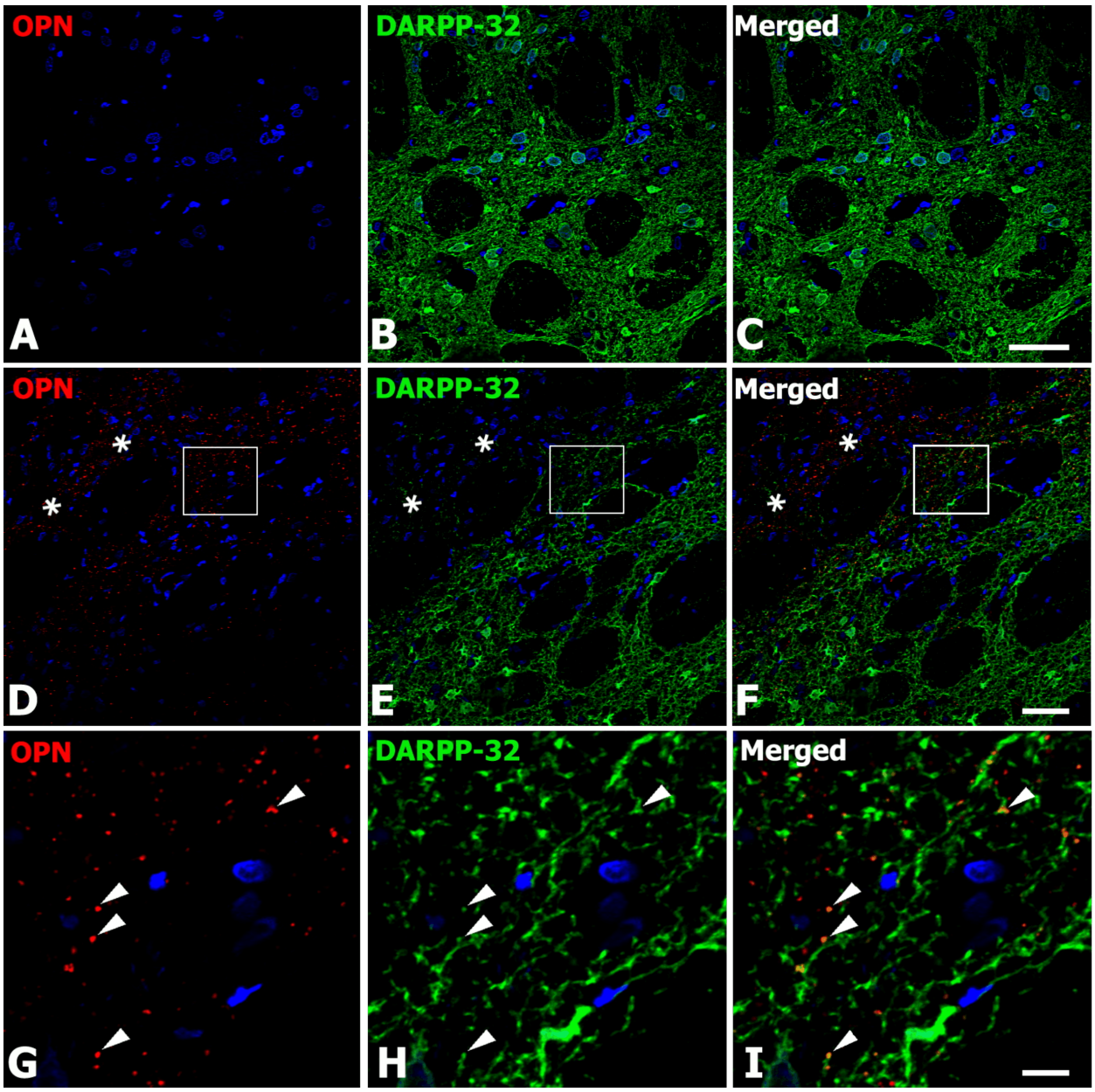

Figure 3 – ***Confocal microscopy analysis of the osteopontin (OPN) expression and the striatal neuronal marker, dopamine and cyclic adenosine monophosphate (cAMP)-regulated neuronal phosphoprotein (DARPP-32). The control sections showed DARPP-32 labeling and no OPN immunolabeling (A–C). The double labeling for OPN and DARPP-32 in the 3-Nitropropionic acid (3NP)-treated rat striatum shows no detectable level of striatal DARPP-32 immunolabeling in damaged areas (asterisks) that show OPN immunolabeling (D–F). High magnifications of the boxed areas (G–I) show the co-localization of some OPN-labeled dots with DARPP-32 (arrowheads) in penumbra. These images show OPN (A, D, and G) and DARPP-32 (B, E, and H) immunoreactivity as well as merged images (C, F, and I) of double immunolabeling. Scale bars: (A–C) 50 µm; (D–F) 30 µm; (G–I) 5 µm.***

We additionally conducted immunoelectron microscopy to examine the distribution of OPN in the degenerated neurons in 3NP-lesioned rats. In the control group, OPN was not detected in the immunoelectron microscopy (Figure 4a). At a higher magnification, ultrastructural examination of striatum from control showed that most mitochondria were small round or oval shape, and have clear cristae (Figure 4b). Scattered OPN-immunoreactive

profiles, which were labeled with electron-dense precipitate, appeared as dot-like shape and they were predominantly distributed in the lesioned core (Figure 4c). At a higher magnification, the labeled profiles could be identified as mitochondria that show a rounded (white arrowhead) or irregularly shaped (arrow) structures, and cristae in the electron micrograph (Figure 4d). Ultrastructural localization of OPN in mitochondria was further analyzed by immunogold/silver methods (Figure 4, e and f). At a higher magnification, a number of silver-enhanced gold particles were localized over the matrix and inner membrane of mitochondria in larger area sizes (Figure 4f). Mitochondria also showed disorganization of cristae and loss of matrix structure.

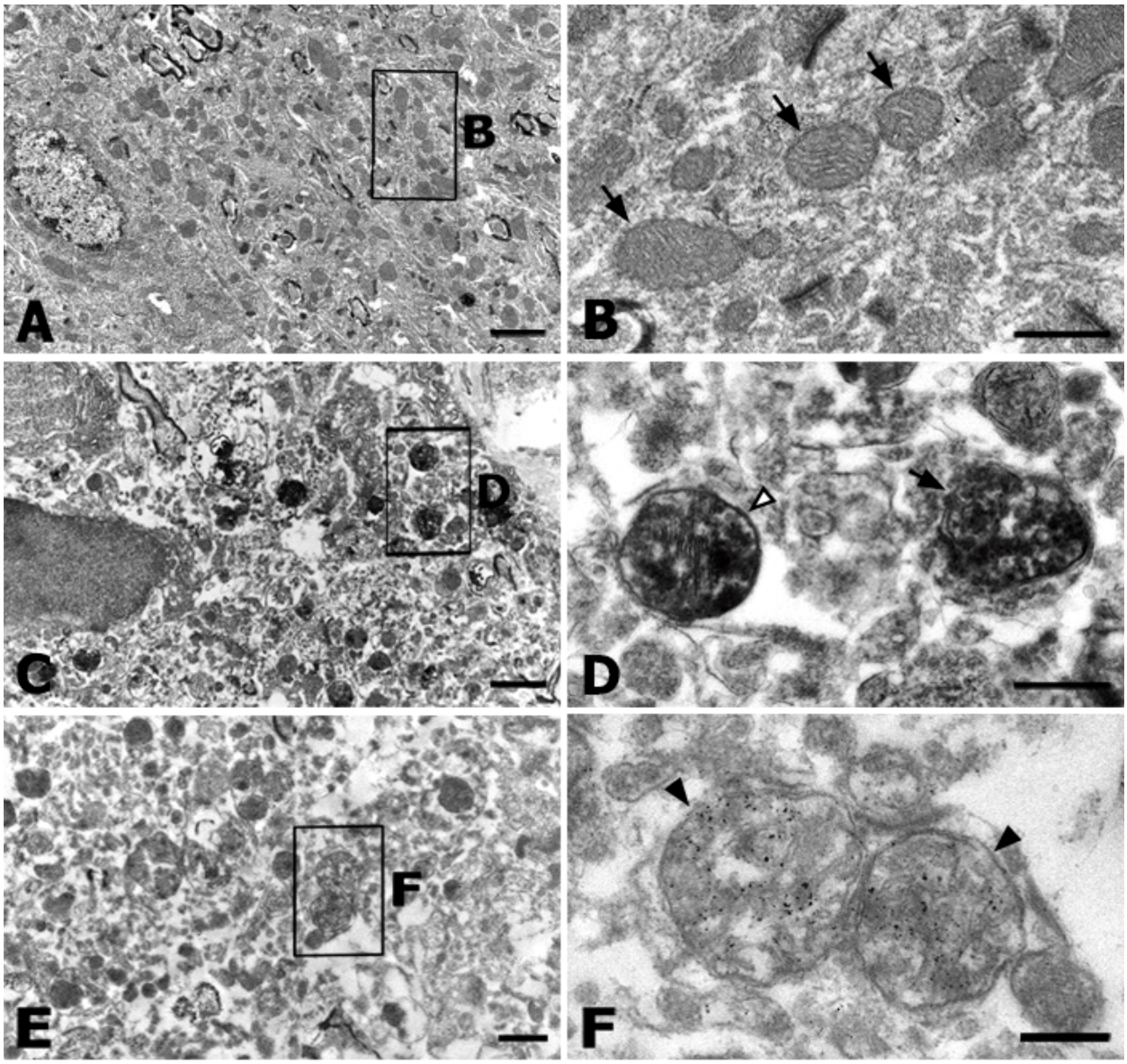

Figure 4 – ***Electron micrographs showing osteopontin (OPN) labeling with immunoperoxidase (A–D) and immuno-gold/silver immunocytochemistry (E and F) in the control striatum and the 3-Nitropropionic acid (3NP)-injured lesion core. OPN expression in control rat striatum is not detected (A and B). (B) Higher magnification of boxed area in (A) show normal mitochondria (arrow) that is round or oval shaped. (C) OPN expression in the 3NP-injured core region appears strongly punctuate. (D) Higher magnification of the boxed area in (C) show that OPN is prominently located in mitochondria, which were the round (white arrowhead) and the irregular (arrow) in shape. (E) Electron microscopic localization of OPN by immunogold/silver immunocytochemistry. (F) Higher magnification of boxed area in (E) show that gold particles for OPN is located within the matrix and inner membrane of swollen mitochondria (arrowhead). Scale bars: (A and C) 1.5 µm; (E) 1 µm; (B and D) 0.5 µm; (F) 0.4 µm.***

Alizarin Red S staining showed that calcium accumulation is markedly increased in the 3NP-treated striatum (Figure 5). Accumulation of calcium and OPN suggest that these parameters are positively correlated in the 3NP-treated striatum. Calcium deposition is important for mitochondrial swelling. To further investigate the correlation between OPN and the calcium precipitate, we measured the area of OPN-labeled mitochondria with immunogold/silver methods. In order to determine whether OPN protein expression was induced in the swollen mitochondria by calcium accumulation, we studied the relationship between the swelling of the mitochondria and OPN expression. The areas of the mitochondria labeled with immunogold are detected by

antibody against OPN and measured by counting the gold particles in the each mitochondrion (Figure 6). In line with the results of OPN immunoreactivity, any immunogold particles were not detected in the control group. In the control group, the average area of mitochondria was 0.124 μm^2. In the 3NP-treated group, counting data of the gold particles can be efficiently used for comparison of OPN expression among mitochondria with different size. There seemed to be a considerable increase in the number of gold particles that were found in the larger and swollen mitochondria compared to the smaller mitochondria (mitochondria within size range 0.1~0.2 μm^2 are used as a standard of comparison). In the hypothesis that the different number of gold particles in the section indicates differences in the level of OPN expression, the present quantitative analysis of gold labeling suggests that the expression level of OPN is closely associated with mitochondrial swelling.

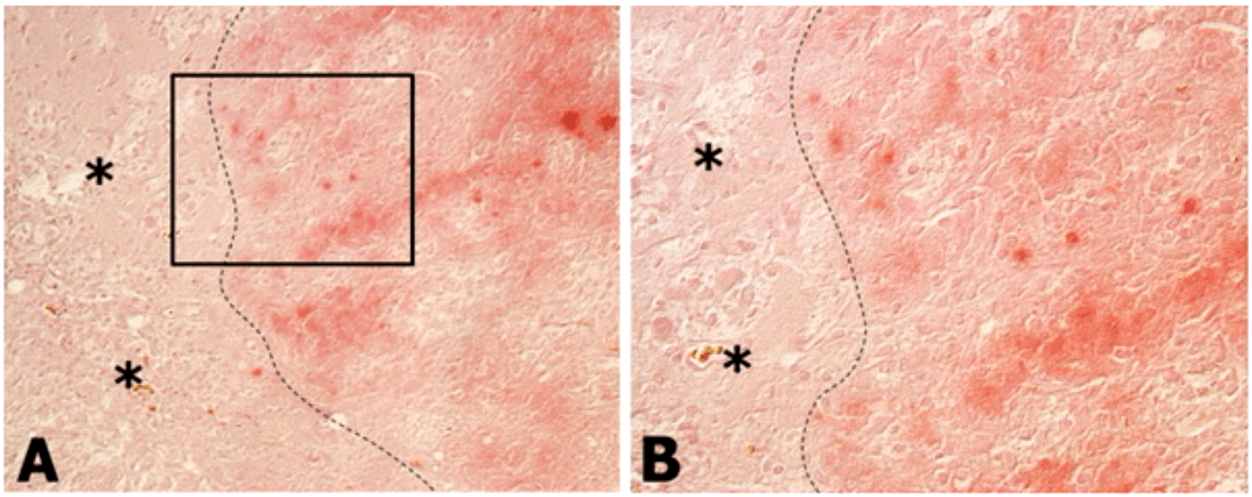

Figure 5 – ***Light microscopy investigation of calcium accumulation. (A) Alizarin Red S staining is restricted to the lesion core (×200). (B) Higher magnification (×400) of the boxed area in (A). The broken line indicates the border between the lesion core and the rim of the lesion (asterisks).***

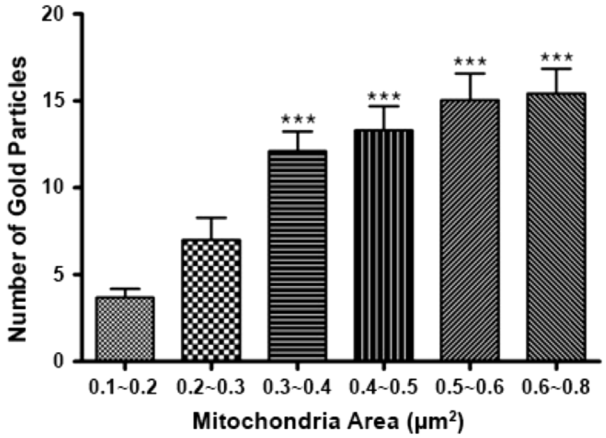

Figure 6 – ***Comparison of the mitochondrial area to osteopontin (OPN) labeled with immunogold particles in the 3-Nitropropionic acid (3NP)-injured lesion core. The number of the gold particles in mitochondria increased with the area size larger. The data are presented as mean ± standard error (SE). ***, p<0.0001 versus unstained mitochondria.***

Discussion

In the present study, we demonstrated that systemic 3NP injection is efficient in modeling striatal degeneration with OPN elevation. The OPN immunoreactivity in the mitochondria of striatal neurons suggests that the mitochondria are important in OPN induction in the 3NP-lesioned core. The mitochondria of striatal neurons are particularly vulnerable to calcium overload-induced MPT [19, 20], and this intracellular calcification disrupts the structural and functional integrity of the organelles [21, 22]. After Alizarin Red S staining, we observed the accumulation of calcium in the 3NP-lesioned core of striatum. MPT, which is the nonselective permeabilization of the inner mitochondrial membrane, is produced by a variety of conditions or compounds. Mirandola *et al.* reported that 3NP treatment was effective on calcium-induced MPT, especially in the mitochondria isolated from heart and brain [20]. Previously, Hamilton & Gould also suggested that glutamate excitotoxicity might play an influential role in the mechanisms of 3NP toxicity [23]. In the recent *in vitro* study, Liot *et al.* demonstrated that 3NP caused mitochondrial fragmentation and neuronal death *via* glutamatergic excitotoxicity [9]. The striatum receives massive excitatory synaptic inputs that are affected by various neurotransmitters such as glutamate and dopamine [24–26]. Therefore, striatal neurons are highly susceptible to excitotoxicity that is induced by increased *N*-methyl-D-aspartate (NMDA) receptor-mediated calcium influx, which results in a rise in cytosolic calcium concentrations [9, 27]. Cytosolic accumulation of calcium, which is associated with a large amount of calcium uptake and oxidative stress of mitochondria, results in the formation of MPT [28, 29]. The swelling of the mitochondria is the most important morphological change resulting from the MPT opening [30, 31]. Synaptic mitochondria, which are spread around the synapse, are more easily exposed to extensive calcium flow and accumulation than non-synaptic mitochondria [32, 33]. Yarana *et al.* reported that synaptic mitochondria isolated from synaptosome showed increase of mitochondrial dysfunction as a result of calcium overload than non-synaptic mitochondria do [34]. Synaptic mitochondria is suggested as associated with a different distribution of the calcium movement

portal pathways, such as the mitochondrial calcium uniporter, mitochondrial ryanodine receptor, and the rapid mode of calcium uptake between synaptic mitochondria and non-synaptic mitochondria [34]. Accordingly, we found more swollen mitochondria with OPN immunoreactivity in dendritic regions than in the cell bodies. Our previous studies also found a correlation between calcium and OPN in ischemic lesions [7, 8].

In our previous studies, we tried to detect calcium in the OPN-immunogold-labeled mitochondria with an electron probe microanalysis. However, we were unable to detect calcium signals. The calcium signals might have been below the threshold for their detection because of alterations in the ionic content and distribution due to chemical fixation and Epon infiltration [35–37]. Even though, still we could not demonstrated the direct link between calcium and OPN change in the 3NP-treated striatum. In the present study, we detected a positive correlation between calcium deposition and OPN-induction by observing the increased pattern of change in the 3NP-lesioned core of striatum. Therefore, in this study, we employed quantifying immunogold labeling that allowed comparison study about concentrations of antigen to determine the relationship between OPN and calcium [38]. As previously mentioned, the swelling of the mitochondria was caused by the excessive levels of calcium that entered the mitochondria space. If OPN was involved in the calcium accumulation, then one would predict an increase in the area of the OPN-stained mitochondria compared to the OPN-unstained mitochondria. Several studies have measured the area of swollen mitochondrial to reveal the effects of diseases and gene mutations on mitochondria [39, 40]. The area of the OPN-labeled mitochondria in the present study was considerably larger than that of the unlabeled mitochondria. Based on this observation, it is conceivable that the abnormal calcium accumulation in the mitochondria is highly correlated with the OPN expression.

Conclusions

Our data demonstrated a correlation between the OPN expression and calcium in the mitochondria of damaged striatal neurons. Although we were not able to directly show the presence of calcium in OPN-stained mitochondria, we were able to produce data that will help us to better understand the mechanisms of OPN expression by measuring the swelling of mitochondria and staining of deposited calcium.

Conflict of interests

The authors declare that they have no conflict of interests.

Author contribution

Hong-Lim Kim and Byung-Joon Chang equally contributed to this manuscript.

HLK, BJC, SMN, SSN, and JHL conceived and conducted experiments, and collected the data. HLK, BJC, SMN, SSN, and JHL analyzed the data. HLK, BJC, and JHL wrote the manuscript. SMN and SSN participated in designing of the study, discussing of results, and revising the manuscript. All authors approved the final version of the manuscript.

Acknowledgments

This research was supported by the faculty research fund of Konkuk University and the Veterinary Science Research Institute of the Konkuk University.

References

[1] Wang KX, Denhardt DT. Osteopontin: role in immune regulation and stress responses. Cytokine Growth Factor Rev, 2008, 19(5–6):333–345.
[2] Liaw L, Almeida M, Hart CE, Schwartz SM, Giachelli CM. Osteopontin promotes vascular cell adhesion and spreading and is chemotactic for smooth muscle cells *in vitro*. Circ Res, 1994, 74(2):214–224.
[3] Liaw L, Birk DE, Ballas CB, Whitsitt JS, Davidson JM, Hogan BL. Altered wound healing in mice lacking a functional osteopontin gene (spp1). J Clin Invest, 1998, 101(7):1468–1478.
[4] Khan SA, Lopez-Chua CA, Zhang J, Fisher LW, Sørensen ES, Denhardt DT. Soluble osteopontin inhibits apoptosis of adherent endothelial cells deprived of growth factors. J Cell Biochem, 2002, 85(4):728–736.
[5] Rangaswami H, Bulbule A, Kundu GC. Osteopontin: role in cell signaling and cancer progression. Trends Cell Biol, 2006, 16(2):79–87.
[6] Sodek J, Ganss B, McKee MD. Osteopontin. Crit Rev Oral Biol Med, 2000, 11(3):279–303.
[7] Park JM, Shin YJ, Kim HL, Cho JM, Lee MY. Sustained expression of osteopontin is closely associated with calcium deposits in the rat hippocampus after transient forebrain ischemia. J Histochem Cytochem, 2012, 60(7):550–559.
[8] Shin YJ, Kim HL, Park JM, Cho JM, Kim CY, Choi KJ, Kweon HS, Cha JH, Lee MY. Overlapping distribution of osteopontin and calcium in the ischemic core of rat brain after transient focal ischemia. J Neurotrauma, 2012, 29(7): 1530–1538.
[9] Liot G, Bossy B, Lubitz S, Kushnareva Y, Sejbuk N, Bossy-Wetzel E. Complex II inhibition by 3-NP causes mitochondrial fragmentation and neuronal cell death *via* an NMDA- and ROS-dependent pathway. Cell Death Differ, 2009, 16(6):899–909.
[10] Borlongan CV, Koutouzis TK, Sanberg PR. 3-Nitropropionic acid animal model and Huntington's disease. Neurosci Biobehav Rev, 1997, 21(3):289–293.
[11] Brouillet E, Condé F, Beal MF, Hantraye P. Replicating Huntington's disease phenotype in experimental animals. Prog Neurobiol, 1999, 59(5):427–468.
[12] Kodsi MH, Swerdlow NR. Mitochondrial toxin 3-nitropropionic acid produces startle reflex abnormalities and striatal damage in rats that model some features of Huntington's disease. Neurosci Lett, 1997, 231(2):103–107.
[13] Kowaltowski AJ, Castilho RF, Vercesi AE. Mitochondrial permeability transition and oxidative stress. FEBS Lett, 2001, 495(1–2):12–15.
[14] Zoratti M, Szabò I. The mitochondrial permeability transition. Biochim Biophys Acta, 1995, 1241(2):139–176.
[15] Brustovetsky N, Brustovetsky T, Jemmerson R, Dubinsky JM. Calcium-induced cytochrome c release from CNS mitochondria is associated with the permeability transition and rupture of the outer membrane. J Neurochem, 2002, 80(2):207–218.
[16] Maciel EN, Kowaltowski AJ, Schwalm FD, Rodrigues JM, Souza DO, Vercesi AE, Wajner M, Castilho RF. Mitochondrial permeability transition in neuronal damage promoted by Ca^{2+} and respiratory chain complex II inhibition. J Neurochem, 2004, 90(5):1025–1035.
[17] Zamzami N, Marchetti P, Castedo M, Decaudin D, Macho A, Hirsch T, Susin SA, Petit PX, Mignotte B, Kroemer G. Sequential reduction of mitochondrial transmembrane potential and generation of reactive oxygen species in early programmed cell death. J Exp Med, 1995, 182(2):367–377.
[18] Kim HL, Lee MY, Shin YJ, Song DW, Park J, Chang BS, Lee JH. Increased expression of osteopontin in the degenerating striatum of rats treated with mitochondrial toxin 3-nitropropionic acid: a light and electron microscopy study. Acta Histochem Cytochem, 2015, 48(5):135–143.
[19] Brustovetsky N, Brustovetsky T, Purl KJ, Capano M, Crompton M, Dubinsky JM. Increased susceptibility of striatal mitochondria to calcium-induced permeability transition. J Neurosci, 2003, 23(12):4858–4867.

[20] Mirandola SR, Melo DR, Saito A, Castilho RF. 3-Nitropropionic acid-induced mitochondrial permeability transition: comparative study of mitochondria from different tissues and brain regions. J Neurosci Res, 2010, 88(3):630–639.
[21] Maetzler W, Stünitz H, Bendfeldt K, Vollenweider F, Schwaller B, Nitsch C. Microcalcification after excitotoxicity is enhanced in transgenic mice expressing parvalbumin in all neurones, may commence in neuronal mitochondria and undergoes structural modifications over time. Neuropathol Appl Neurobiol, 2009, 35(2):165–177.
[22] Nitsch C, Scotti AL. Ibotenic acid-induced calcium deposits in rat substantia nigra. Ultrastructure of their time-dependent formation. Acta Neuropathol, 1992, 85(1):55–70.
[23] Hamilton BF, Gould DH. Nature and distribution of brain lesions in rats intoxicated with 3-nitropropionic acid: a type of hypoxic (energy deficient) brain damage. Acta Neuropathol, 1987, 72(3):286–297.
[24] Cepeda C, Levine MS. Dopamine and N-methyl-D-aspartate receptor interactions in the neostriatum. Dev Neurosci, 1998, 20(1):1–18.
[25] Jakel RJ, Maragos WF. Neuronal cell death in Huntington's disease: a potential role for dopamine. Trends Neurosci, 2000, 23(6):239–245.
[26] Nishino H, Hida H, Kumazaki M, Shimano Y, Nakajima K, Shimizu H, Ooiwa T, Baba H. The striatum is the most vulnerable region in the brain to mitochondrial energy compromise: a hypothesis to explain its specific vulnerability. J Neurotrauma, 2000, 17(3):251–260.
[27] Albin RL, Greenamyre JT. Alternative excitotoxic hypotheses. Neurology, 1992, 42(4):733–738.
[28] Crompton M. The mitochondrial permeability transition pore and its role in cell death. Biochem J, 1999, 341(Pt 2):233–249.
[29] Vercesi AE, Kowaltowski AJ, Oliveira HC, Castilho RF. Mitochondrial Ca^{2+} transport, permeability transition and oxidative stress in cell death: implications in cardiotoxicity, neurodegeneration and dyslipidemias. Front Biosci, 2006, 11:2554–2564.
[30] Bernardi P. The permeability transition pore. Control points of a cyclosporin A-sensitive mitochondrial channel involved in cell death. Biochim Biophys Acta, 1996, 1275(1–2):5–9.
[31] Friberg H, Wieloch T. Mitochondrial permeability transition in acute neurodegeneration. Biochimie, 2002, 84(2–3):241–250.
[32] Banaclocha MM, Hernández AI, Martínez N, Ferrándiz ML. N-acetylcysteine protects against age-related increase in oxidized proteins in mouse synaptic mitochondria. Brain Res, 1997, 762(1–2):256–258.
[33] Martinez M, Hernández AI, Martínez N, Ferrándiz ML. Age-related increase in oxidized proteins in mouse synaptic mitochondria. Brain Res, 1996, 731(1–2):246–248.
[34] Yarana C, Sanit J, Chattipakorn N, Chattipakorn S. Synaptic and nonsynaptic mitochondria demonstrate a different degree of calcium-induced mitochondrial dysfunction. Life Sci, 2012, 90(19–20):808–814.
[35] Bordat C, Bouet O, Cournot G. Calcium distribution in high-pressure frozen bone cells by electron energy loss spectroscopy and electron spectroscopic imaging. Histochem Cell Biol, 1998, 109(2):167–174.
[36] Consort Ribeiro K, Benchimol M, Farina M. Contribution of cryofixation and freeze-substitution to analytical microscopy: a study of *Tritrichomonas* foetus hydrogenosomes. Microsc Res Tech, 2001, 53(1):87–92.
[37] Nagata T. X-ray microanalysis of biological specimens by high voltage electron microscopy. Prog Histochem Cytochem, 2004, 39(4):185–319.
[38] D'Amico F, Skarmoutsou E. Quantifying immunogold labelling in transmission electron microscopy. J Microsc, 2008, 230(Pt 1):9–15.
[39] Darios F, Corti O, Lücking CB, Hampe C, Muriel MP, Abbas N, Gu WJ, Hirsch EC, Rooney T, Ruberg M, Brice A. Parkin prevents mitochondrial swelling and cytochrome c release in mitochondria-dependent cell death. Hum Mol Genet, 2003, 12(5):517–526.
[40] Sisková Z, Mahad DJ, Pudney C, Campbell G, Cadogan M, Asuni A, O'Connor V, Perry VH. Morphological and functional abnormalities in mitochondria associated with synaptic degeneration in prion disease. Am J Pathol, 2010, 177(3):1411–1421.

Corresponding author
Jong-Hwan Lee, Professor, DVM, PhD, Department of Anatomy, College of Veterinary Medicine and Veterinary Science Research Institute, Konkuk University, 120 Neungdong-ro, Gwangjin-gu, 05030 Seoul, South Korea; Phone +82 2 450 4209, Fax +82 2 450 3037, e-mail: jhlee21@konkuk.ac.kr

Received: June 16, 2017

Accepted: February 7, 2018